Low-temperature physical properties and electronic structures of Ni_3Sb, Ni_5Sb_2, $NiSb_2$, and NiSb *

Luo Xiao-Ning(罗肖宁)[a)b)], Dong Cheng(董 成)[b)†], Liu Shi-Kai(刘世凯)[a)], Zhang Zi-Ping(张子平)[a)], Li Ao-Lei(李傲雷)[b)], Yang Li-Hong(杨立红)[b)], and Li Xiao-Chuan(李晓川)[b)]

[a)] *School of Material Science and Engineering, Henan University of Technology, Zhengzhou* 450001, *China*
[b)] *National Laboratory for Superconductivity, Institute of Physics, Chinese Academy of Sciences, Beijing* 100190, *China*

(Received 19 January 2015; revised manuscript received 6 February 2015; published online 10 April 2015)

We report the results of low temperature resistivity and magnetization measurements on polycrystalline samples of four Ni–Sb compounds, Ni_3Sb, Ni_5Sb_2, NiSb, and $NiSb_2$. Resistivity measurements revealed that these compounds exhibit a metallic type of electrical conductivity. Temperature dependences of the resistivities were well fitted by the generalized Bloch–Grüneisen formula with an exponent of $n = 3$, indicating that the s–d interband scattering is the dominant scattering mechanism. The magnetic susceptibilities of Ni_5Sb_2, NiSb, and $NiSb_2$ are almost independent of temperature (above 150 K), exhibiting Pauli paramagnetic behavior. The temperature dependences of the susceptibilities were fitted using the Curie–Weiss law. Ni_3Sb was found to have a paramagnetic–ferromagnetic phase transition at 229 K.

First-principles calculations have been performed to investigate the electronic structures and physical properties of these Ni–Sb alloys. The calculation of the band structure predicted that Ni_3Sb, Ni_5Sb_2, NiSb, and $NiSb_2$ have characteristics of metal, and the ground state of Ni_3Sb is ferromagnetic. The electrical and magnetic properties observed experimentally are consistent with that predicted by the first-principle electronic structure calculations.

Keywords: Ni–Sb alloys, resistivity, susceptibility, electronic structure

PACS: 72.15.Eb, 75.20.En, 71.20.Be **DOI:** 10.1088/1674-1056/24/6/067201

1. Introduction

Since the superconductivity of $LnNi_2B_2C$ (*Ln* = Y, Tm, Er, Ho or Lu)[1,2] has been discovered, extensive studies were performed successfully in the search for new Ni-based superconductors. In 2001, a new superconductor $MgCNi_3$[3] with an antiperovskite structure was found with T_c around 8 K. Subsequently, superconductivity was also found in $CdCNi_3$,[4] $ZnNNi_3$,[5] and $CuNNi_3$[6] with the antiperovskite structure. Several Ni-based superconductors with the '1111'-type structure, such as LaONiP,[7,8] LaNiOAs,[9] and $LaNiBiO_{1-x}$,[10] were found soon after the discovery of superconductivity in LaOFeP.[11] In addition, $CeNi_{0.8}Bi_2$[12] and $LaNi_{0.9}Bi_2$[13] are superconductors and they share the same space group with the '1111'-type structure.[14]

Though all the Ni-based superconductors mentioned above are ternary or quaternary phases, we noticed that some binary nickel alloys are also superconductors. For example, both NiBi and $NiBi_3$ are superconductors,[15,16] and they are the only two intermediate phases in the Ni–Bi system.[17] Because Sb and Bi belong to the same group in the periodic table, we conjectured that some Ni–Sb binary phases might be superconductor as well. In this paper, we investigate the electrical and magnetic properties of the Ni–Sb alloys at low temperature to search for possible superconductors in the Ni–Sb system.

Four intermediate phases, Ni_3Sb, Ni_5Sb_2, NiSb, and $NiSb_2$, exist in the Ni–Sb binary system near room temperature.[18,19] The Ni_3Sb, NiSb, and $NiSb_2$ phases crystallize with the well-known Cu_3Ti, NiAs, and FeS_2 type structure respectively, whereas Ni_5Sb_2 crystallizes in a unique type of structure.[20–22] There is very scarce information in the literature about their low-temperature physical properties. The high-temperature phase of Ni_3Sb attracted a great deal of attention, because Ni atoms of this alloy possess the highest mobility ever observed in a metallic system.[23] Bulk NiSb and nanosized Ni_5Sb_2, NiSb, and $NiSb_2$ have been studied as promising electrode materials in lithium-ion batteries recently.[24–27] To the best of our knowledge, only the low-temperature resistivity and susceptibility of NiSb were studied previously. NiSb was found to be a typical Pauli paramagnetic metal by resistivity and susceptibility measurements.[28,29] Besides, we have incomplete information about the physical properties of $NiSb_2$. The bulk $NiSb_2$ shows metallic behavior by electric resistivity measurement above room temperature.[30] $NiSb_2$ nanocrystals are ferromagnetic.[31] At present, knowledge about the low-temperature physical properties of Ni_3Sb and Ni_5Sb_2 is obviously lacking.

The main aim of the present work is to investigate the low-temperature electrical and magnetic properties of Ni_3Sb, Ni_5Sb_2, NiSb, and $NiSb_2$. We also performed the first-principle electronic structure calculations for these compounds

*Project supported by the National Natural Science Foundation of China (Grant No. 21271183) and the National Basic Research Program of China (Grant Nos. 2011CBA00112 and 2011CB808202).

†Corresponding author. E-mail: chengdon@aphy.iphy.ac.cn

© 2015 Chinese Physical Society and IOP Publishing Ltd

in order to elucidate their physical properties.

2. Experimental and computational method

The polycrystalline samples of Ni_3Sb, Ni_5Sb_2, $NiSb_2$, and NiSb were synthesized at high temperature from nickel (99.999%, Sinapharm) and antimony (99.999%, Sinapharm) powders. Stoichiometric amounts of Ni and Sb powders were mixed and pressed into pellets. The pellets were sealed in evacuated quartz tubes. The samples were placed into a furnace and heated at 1050 °C for 24 h, and then cooled down to 600 °C and annealed at this temperature for 100 hours. Finally, the samples were furnace-cooled to room temperature. The powder x-ray diffraction data of the samples were collected on a Rigaku D/max-Ultima IV diffractometer with Cu K_α radiation at room temperature. The 2θ scan range was from 10° to 120°. The lattice parameters of the samples were calculated using the least-square method with the help of the PowderX program.[32] The grain morphology of the samples was examined using a scanning electron microscope (FE-SEM, Hitachi S4800), and the chemical compositions were analyzed by an energy-dispersive x-ray spectroscopy (EDX) attachment. The electrical resistivity measurement was performed using the conventional four-probe method. The temperature dependence of the magnetization was measured at a magnetic field of 1 T using a Quantum Design MPMS XL-5 SQUID magnetometer in the temperature range from 5 K to 300 K.

We employed the CASTEP (Cambridge Serial Total Energy Package) program[33] for the electronic structure calculations. The spin-polarized generalized gradient approximation with the Perdew–Burke–Ernzerhof (PBE) scheme is adopted for the exchange–correlation potential.[34] The ultrasoft pseudopotentials[35] with a plane wave cutoff energy of 330 eV were used for the calculations of Ni_3Sb, $NiSb_2$, and NiSb, and the norm-conserving pseudopotential[36] is used for Ni_5Sb_2 with cutoff energy of 860 eV. The Brillouin zone was sampled with a 5×6×6, 5×4×7, 7×7×6, 2×5×4 Monkhorst–Pack grid for Ni_3Sb, Ni_5Sb_2, $NiSb_2$, and NiSb, respectively. The crystal structure data in references listed in Table 1 were used for the calculations.

3. Results and discussion

3.1. Powder x-ray diffraction and microanalysis

The powder x-ray diffraction data indicate that all samples are single phase. Figure 1 shows the x-ray power diffraction patterns of the Ni_3Sb, Ni_5Sb_2, $NiSb_2$, and NiSb samples. All observed peaks in each pattern can be indexed to the previously reported structure with the lattice parameters listed in Table 1. The lattice parameters given in the reference papers are also listed in Table 1 for comparison. Our results are consistent with those reported in the literature.

The elemental compositions of the samples determined by EDX analysis are listed in Table 2. The measured elemental compositions are consistent with the stoichiometric ones within the experimental errors.

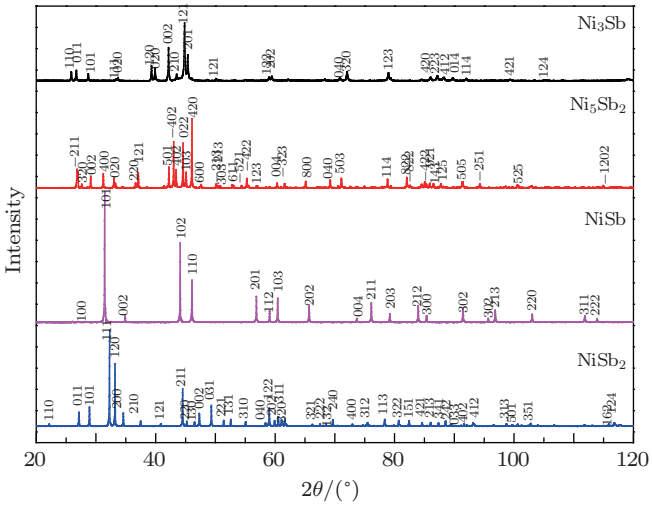


Fig. 1. (color online) Powder XRD patterns of Ni_3Sb, Ni_5Sb_2, NiSb, and $NiSb_2$ samples.

Table 1. Summary of lattice parameters measured in this work and previous works.

Sample	This work				Previous works				Reference
	a/Å	*b*/Å	*c*/Å	β/(°)	*a*/Å	*b*/Å	*c*/Å	β/(°)	
Ni_3Sb	4.5161(3)	5.3155(3)	4.2831(3)	90	4.519	5.317	4.277	90	[37]
Ni_5Sb_2	11.4543(3)	5.4261(2)	6.1326(3)	90.51(3)	11.4568	5.4271	6.1349	90.53	[21]
NiSb	3.9360(1)	3.9360(1)	5.1382(1)	90	3.935	3.935	5.136	90	[38]
$NiSb_2$	5.1841(1)	6.3173(1)	3.8400(1)	90	5.1837	6.3184	3.8408	90	[39]

Table 2. Elemental compositions determined by EDX analysis.

Sample	Ni_3Sb	Ni_5Sb_2	NiSb	$NiSb_2$
Ni/at%	74.6	71.7	51.0	33.1
Sb/at%	25.4	28.3	49.0	66.9

The SEM micrographs of the Ni_3Sb, Ni_5Sb_2, NiSb, and $NiSb_2$ samples are shown in Fig. 2. The Ni_3Sb, Ni_5Sb_2, and $NiSb_2$ samples are aggregations of irregular-shaped particles with sizes in the range of 5 μm–20 μm. The micrographs also revealed the presence of porosity in the Ni_3Sb, Ni_5Sb_2, and $NiSb_2$ samples. The NiSb sample has the most regular morphology among all the samples, which may be explained in terms of the phase transitions. Only NiSb has no phase transition below 1000 °C.[18] It can be seen from Fig. 2(c) that some of the NiSb grains clearly show hexagonal facets, signifying their hexagonal crystal structure. The grain sizes of the

NiSb sample are varied from 10 μm to about 25 μm.

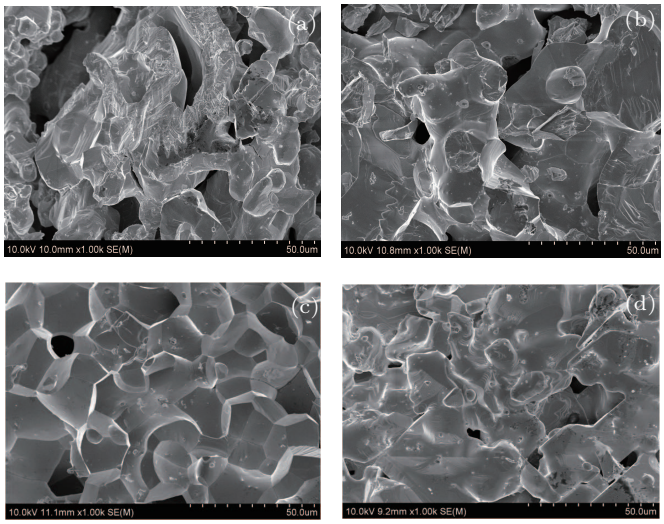


Fig. 2. SEM micrographs of the Ni_3Sb (a), Ni_5Sb_2 (b), NiSb (c), and $NiSb_2$ (d) samples.

3.2. Electronic structure

Figure 3 shows the calculated band structures and densities of states (DOS) for Ni_3Sb, Ni_5Sb_2, NiSb, and $NiSb_2$. A common feature of these band structures is the bands crossing at the Fermi level along various directions, which results in finite DOS at the Fermi level. Hence, these compounds are predicted to exhibit metallic behavior by the electronic structure calculations, which is in accordance with our experimental results given in the next sections. The total DOSs at the Fermi levels $N(E_F)$ are 9.987, 14.561, 2.088, and 2.477 (states/eV) for Ni_3Sb, Ni_5Sb_2, NiSb, and $NiSb_2$, respectively. Since the valence configurations of isolated atoms are $3d^84s^2$ for nickel and $5s^25p^3$ for antimony, the electron bands near the Fermi levels will be occupied by these valence electrons. In addition to the total DOS, the partial densities of s, p, and d states are also illustrated in Fig. 3. We note that the p and d states make the dominating contribution to the total DOS near the Fermi levels. At the Fermi levels, the partial densities of d states provide over half of the total DOS in the Ni-rich phases (Ni_3Sb, Ni_5Sb_2, and NiSb). Even in the Sb-rich $NiSb_2$ phase, the partial densities of d states account for more than one-third of the total DOS. These calculation results support the s–d scattering mechanism responsible for the resistivity in these alloys (described in the next section).

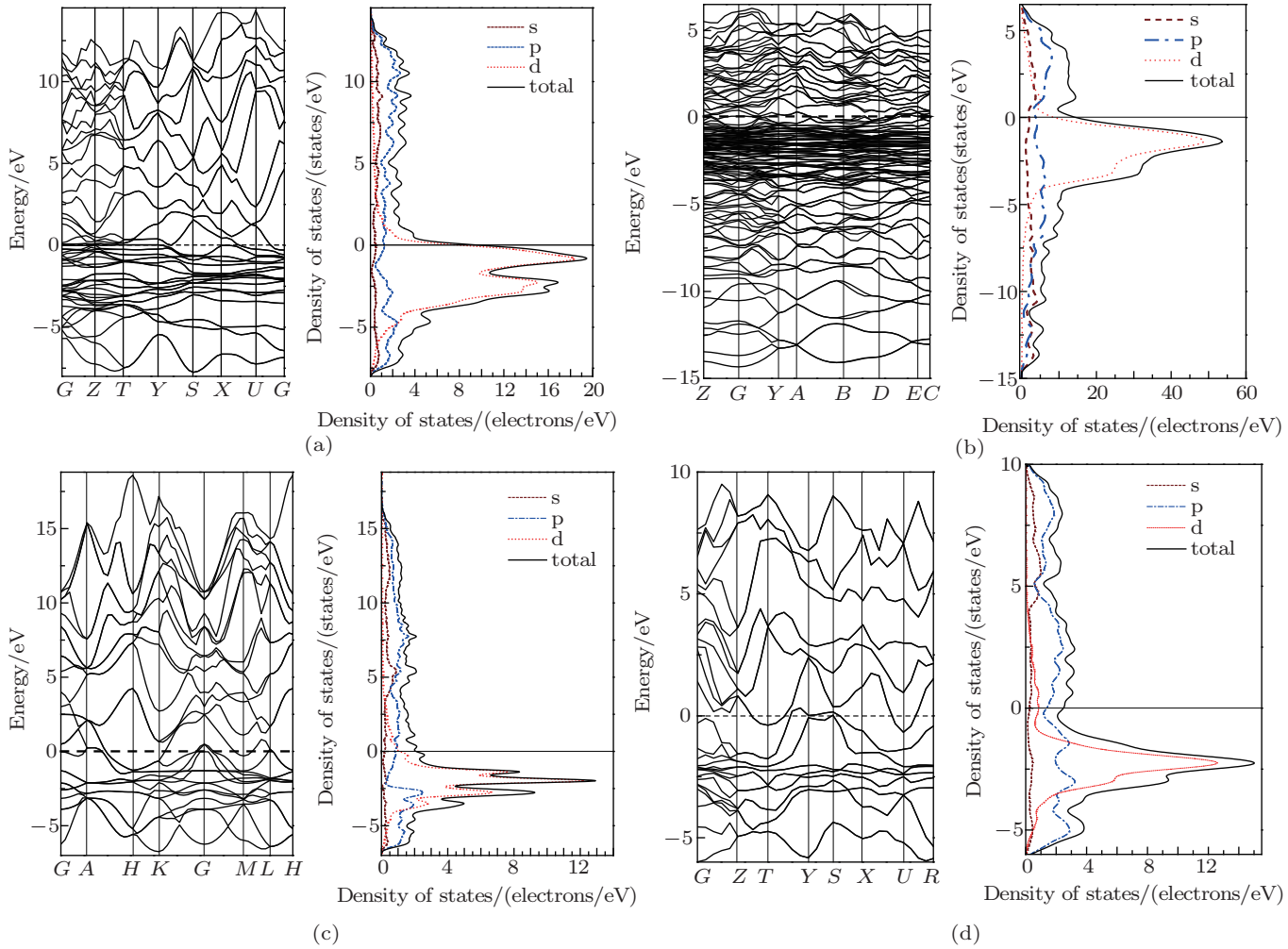


Fig. 3. (color online) The calculated band structure (left) and total densities of states and the partial densities of s, p, and d states (right) for Ni_3Sb (a), Ni_5Sb_2 (b), NiSb (c), and $NiSb_2$ (d). The horizontal line denotes the position of the Fermi energy, which has been chosen to be 0 eV.

The spin-polarized electron structure calculations have also provided valuable information for the magnetic properties. The calculated total magnetic moment is $0.36\mu_B$ per cell for Ni_3Sb in the ground state. Therefore, Ni_3Sb should be ferromagnetic. The calculated total magnetic moments are practically zero for Ni_5Sb_2, NiSb, and $NiSb_2$. Hence, Ni_5Sb_2, NiSb, and $NiSb_2$ were predicted to be paramagnetic by the theoretical calculations.

3.3. Electrical resistivity

In Fig. 4 we plot the temperature dependence of resistivity of the samples. All samples exhibit metallic behavior and the resistivities increase linearly with temperature above 50 K. No superconductivity was found down to 2 K.

The temperature dependence of the resistivities was modeled by the generalized Bloch–Grüneisen formula,[40–42]

$$\rho(T) = \rho_0 + C\left(\frac{T}{\theta_D}\right)^n \int_0^{\theta_D/T} \frac{Z^n}{(e^z-1)(1-e^{-z})}\mathrm{d}z, \qquad (1)$$

where ρ_0 is the residual resistivity due to the temperature-independent scattering from defects and impurities. C is a prefactor that is related to the electron–phonon coupling strength. θ_D is the Debye temperature. The exponent n is dependent on the dominant scattering mechanisms, and takes the value of 5 for electron–phonon intraband scattering and 3 for electron–phonon s–d interband scattering. The s–d interband scattering is significant in alloys with an unfilled d band.

We calculated by a least-squares fit to the data using Eq. (1) for both values of n. A better fit to the experimental data was obtained with $n = 3$ (solid line in Fig. 4.) than that with $n = 5$ for each sample, indicating that s–d interband scattering is the dominant scattering mechanism in all these compounds. This can be explained with our band structure calculation results as they all have an unfilled d-band.

The residual resistivity (ρ_0), the prefactor (C), and the Debye temperature (θ_D), obtained from the fits of the resistivity data are summarized in Table 3. The residual resistivity monotonically increases with the Ni content, indicating that the Ni-rich samples contain more defects and impurities.

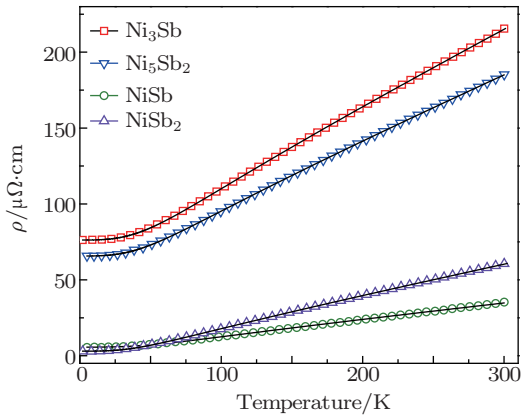


Fig. 4. (color online) Temperature dependence of electrical resistivity of Ni_3Sb, Ni_5Sb_2, NiSb, and $NiSb_2$. The small symbols denote the experimental data points, and the solid lines represent the fits using Eq. (1). Note that the experimental data points are rarefied for a better clarity.

Table 3. The residual resistivity (ρ_0), Debye temperature (θ_D), and the prefactor (C) obtained from the fits of the resistivity data using Eq. (1).

Sample	C/μΩ·cm	ρ_0/μΩ·cm		θ_D/K
Ni_3Sb	76. 215	310		199. 90
Ni_5Sb_2	65. 702	300		248. 73
NiSb	5. 65	330		67. 32
$NiSb_2$	3. 00	275		108. 78

3.4. Magnetic properties

Figure 5 shows the temperature dependences of the magnetic susceptibility for the samples. The magnetic susceptibility data were measured in the field cooling (FC) and zero-field cooling (ZFC) modes. Only the FC data are displayed in Fig. 5 as the ZFC data nearly coincide with the ZC ones. It can be seen in Fig. 5 that Ni_3Sb shows a paramagnetic–ferromagnetic phase transition around 230 K. The magnetic susceptibilities of Ni_5Sb_2, $NiSb_2$, and NiSb are almost independent of temperature above 150 K, showing Pauli paramagnetic behavior as expected by our electronic structure calculations. The upturns of the susceptibilities in the low temperature region are attributable to the effect of paramagnetic impurities or paramagnetic surface states.[29,43] There is a small kink around 275 K in the susceptibility of Ni_5Sb_2, which might be caused by a trace amount of ferromagnetic impurities.

We have fit the magnetic susceptibility data to a modified Curie–Weiss law,

$$\chi(T) = \chi_0 + C/(T-\theta), \qquad (2)$$

where C is the paramagnetic Curie constant, θ is the Curie–Weiss temperature which represents the magnetic exchange interactions between the spins, and χ_0 is the temperature-independent susceptibility. The solid lines in Fig. 5 are fits to the modified Curie–Weiss law. The related parameters obtained from the fits are listed in Table 4. The Curie temperature of Ni_3Sb was determined to be 229 K from the fit. The temperature intercept of $(\chi_0-\chi_0)^{-1}$ versus the T plot (the inset in Fig. 5(a)) also gives the same Curie temperature.

In the Ni–Sb alloys, the Pauli paramagnetism of the conduction electrons makes a major contribution to χ_0. Since the Pauli paramagnetic susceptibility is proportional to the DOS at the Fermi levels $N(E_F)$, the χ_0 values from the fitting analysis have the same variation trend with the calculated $N(E_F)$. The negative values of the Curie temperature for Ni_5Sb_2, $NiSb_2$, and NiSb suggest the presence of weak antiferromagnetic exchange interactions. The Curie constant $C = N\mu^2/3k_B$ is a measure of the paramagnetic ion concentration, (N = number of magnetic ions/mol, μ = magnetic moment of the ion, and k_B = Boltzmann's constant). Assuming the magnetic ions were Ni^{2+} (with spin-only effective magnetic moment $\mu = 2.83\ \mu_B$), the Ni^{2+} concentrations derived from the Curie constants are less than 1.5 ppb in the Ni_5Sb_2, $NiSb_2$, and NiSb samples.

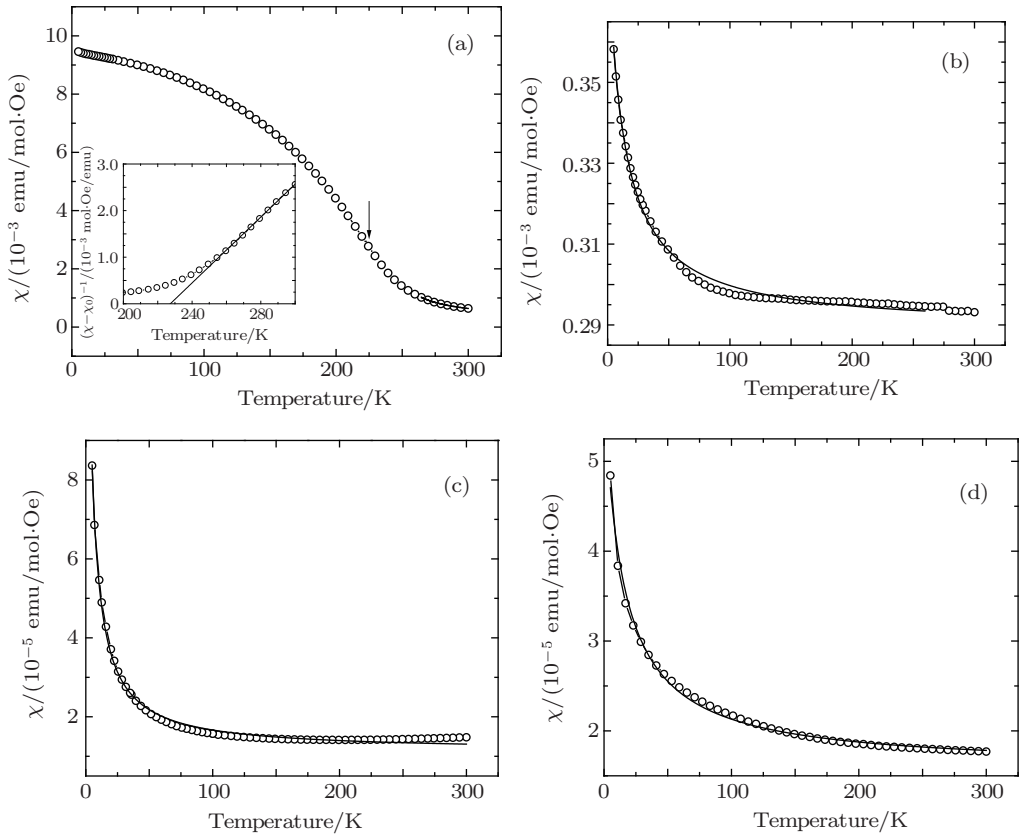


Fig. 5. Temperature dependence of the magnetic susceptibility χ of Ni_3Sb (a), Ni_5Sb_2 (b), NiSb (c), and $NiSb_2$ (d) measured with an applied field of 1 T. The measured data points are presented as unfilled circles. The solid lines are fits to the modified Curie–Weiss law with parameters given in Table 4. The arrow in Fig. 5(a) indicates the Curie temperature determined from the fit. The inset in Fig. 5(a) shows the $(\chi-\chi_0)^{-1}$ versus the T plot for Ni_3Sb. The unit 1 Oe = 79.5775 A·m^{-1}.

Table 4. Susceptibility parameters obtained from fits using Eq. (2).

Sample	$\chi_0/(10^{-3}$ emu/mol·Oe)	$C/(10^{-3}$ K·emu/mol·Oe)	θ/K
Ni_3Sb	0.255	27	229
Ni_5Sb_2	0.289	1.20	–12.3
NiSb	0.011	0.55	–2.6
$NiSb_2$	0.015	0.70	–19. 0

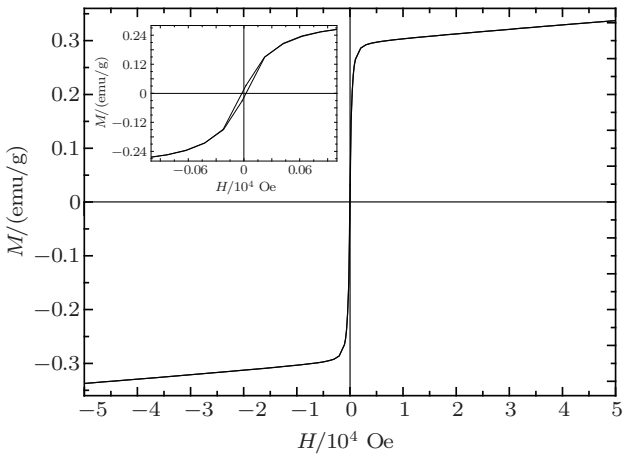


Fig. 6. Magnetization hysteresis loop for the Ni_3Sb sample measured at 50 K. The inset shows an enlarged portion of the loop in the vicinity of zero fields.

To confirm the ferromagnetism of Ni_3Sb after the magnetic phase transition, the magnetization versus magnetic field curve of the Ni_3Sb sample was measured at 50 K with an applied field in the range of −5 T to 5 T. The obtained curve is shown in Fig. 6. Ni_3Sb at 50 K is obviously ferromagnetic for the magnetization versus magnetic field curve showing a well-defined hysteresis loop. The coercive field (H_c), the saturated magnetization (M_s), and the remnant magnetization (M_{rem}) were determined to be $H_c = 22$ Oe, $M_s = 0.337$ emu/g, and $M_{rem} = 0.0163$ emu/g. Therefore, we can conclude that Ni_3Sb has weak ferromagnetism below the Curie temperature 229 K. The ferromagnetism of Ni_3Sb at low temperature is consistent with the prediction from the first-principle electronic structure calculations.

4. Conclusions

In order to search for possible superconductors in the Ni–Sb binary alloys, we measured the low-temperature electrical resistivities and susceptibilities of Ni_3Sb, Ni_5Sb_2, $NiSb_2$, and NiSb polycrystalline samples and calculated their electronic structures. They exhibit a metallic type of electrical conductivity, and the s–d interband scattering is the dominant scattering mechanism responsible to their electrical resistivity. Ni_5Sb_2, $NiSb_2$, and NiSb are found to be Pauli paramagnetic metals.

The upturns of their susceptibilities in the low temperature region are attributable to the effect of paramagnetic impurities or paramagnetic surface states. Ni_3Sb has a paramagnetic–ferromagnetic phase transition at 229 K. The electrical and magnetic properties observed experimentally are consistent with those predicted by the first principle calculations. Although no superconductivity has been found down to 2 K in these binary Ni–Sb compounds, we believe that more superconductors will be found in ternary and multi-elements systems containing Ni and Sb.

References

[1] Cava R J, Takagi H, Zandbergen H W, Krajewski J J, Peck W F, Siegrist T, Batlogg B, Vandover R B, Felder R J, Mizuhashi K, Lee J O, Eisaki H and Uchida S 1994 *Nature* **367** 252

[2] Sinha S, Lynn J, Grigereit T, Hossain Z, Gupta L, Nagarajan R and Godart C 1995 *Phys. Rev. B* **51** 681

[3] He T, Huang Q, Ramirez A P, Wang Y, Regan K A, Rogado N, Hayward M A, Haas M K, Slusky J S, Inumara K, Zandbergen H W, Ong N P and Cava R J 2001 *Nature* **411** 54

[4] Uehara M, Yamazaki T, Kôri T, Kashida T, Kimishima Y and Hase I 2007 *J. Phys. Soc. Jpn.* **76** 034714

[5] Uehara M, Uehara A, Kozawa K and Kimishima Y 2009 *J. Phys. Soc. Jpn.* **78** 033702

[6] He B, Dong C, Yang L H, Chen X C, Ge L H, Mu L B and Shi Y G 2013 *Supercond. Sci. Technol.* **26** 125015

[7] Watanabe T, Yanagi H, Kamiya T, Kamihara Y, Hiramatsu H, Hirano M and Hosono H 2007 *Inorg. Chem.* **46** 7719

[8] Tegel M, Bichler D and Johrendt D 2008 *Solid State Sci.* **10** 193

[9] Watanabe T, Yanagi H, Kamihara Y, Kamiya T, Hirano M and Hosono H 2008 *J. Solid State Chem.* **181** 2117

[10] Buckow A, Retzlaff R, Kurian J and Alff L 2012 *Phys. Procedia* **27** 300

[11] Kamihara Y, Hiramatsu H, Hirano M, Kawamura R, Yanagi H, Kamiya T and Hosono H 2006 *J. Am. Chem. Soc.* **128** 10012

[12] Kodama K, Wakimoto S, Igawa N, Shamoto S, Mizoguchi H and Hosono H 2011 *Phys. Rev. B* **83** 214512

[13] Kurian J, Buckow A, Retzlaff R and Alff L 2013 *Physica C* **484** 171

[14] Flandorfer H, Sologub O, Godart C, Hiebl K, Rogl P and Ndl H 1996 *Solid State Commun.* **97** 561

[15] Matthias B T 1953 *Phys. Rev.* **92** 874

[16] Fujimori Y, Kan S I, Shinozaki B and Kawaguti T 2000 *J. Phys. Soc. Jpn.* **69** 3017

[17] Vassilev G P R J and Wnuk G 2007 *Int. J. Mater. Res.* **98** 468

[18] Zhang Y, Li C, Du Z and Guo C 2008 *Calphad* **32** 378

[19] Minić D, Manasijević D, Ćsovic V, Todorović A, Dervišević I, Živković D and Dokić J 2011 *Calphad* **35** 308

[20] Le Clanche M C, Députier S, Jégaden J C, Guérin R, Ballini Y and Guivarc'h A 1994 *J. Alloys Compd.* **206** 21

[21] Heinrich S, Rexer H U and Schubert K 1978 *J. Less Common Met.* **60** 65

[22] Naud J and Parijs D 1972 *Mater. Res. Bull.* **7** 301

[23] Randl O G, Vogl G, Kaisermayr M, Buhrer W, Petry W and Pannetier J 1996 *J. Phys.: Condens. Matter* **8** 7689

[24] Villevieille C, Ionica-Bousquet C M, Ducourant B, Jumas J C and Monconduit L 2007 *J. Power Sources* **172** 388

[25] Yang Y W, Li T Y, Liu F, Zhu W B, Li X L, Wu Y C and Kong M G 2013 *Microelectron. Eng.* **104** 1

[26] Xie J, Zhao X B, Yu H M, Qi H, Cao G S and Tu J P 2007 *J. Alloys Compd.* **441** 231

[27] Xie J, Zhao X B, Cao G S, Zhao M J and Su S F 2005 *J. Alloys Compd.* **393** 283

[28] Chen T, Rogowski D and White R 1978 *J. Appl. Phys.* **49** 1425

[29] Kobayashi H, Kageshima M, Kimura N, Aoki H, Oohigashi M, Motizuki K and Kamimura T 2004 *J. Magn. Magn. Mater.* **272** E247

[30] Liu K G, Ji N J and Ma Z Q 2012 *Adv. Mater. Res.* **503** 507

[31] Li C, Hu J, Peng Q and Wang X 2008 *Mater. Chem. Phys.* **110** 106

[32] Dong C 1999 *J. Appl. Crystallogr.* **32** 838

[33] Clark S J, Segall M D, Pickard C J, Hasnip P J, Probert M I, Refson K and Payne M C 2005 *Z. Kristallogr.* **220** 567

[34] Perdew J P, Burke K and Ernzerhof M 1996 *Phys. Rev. Lett.* **77** 18

[35] Vanderbilt D 1990 *Phys. Rev. B* **41** 7892

[36] Hamann D, Schlüter M and Chiang C 1979 *Phys. Rev. Lett.* **43** 1494

[37] Naud J and Parijs D 1972 *Mater. Res. Bull.* **4** 301

[38] Le Clanche M C, Deputier S, Jégaden J C, Guérin R, Ballini Y and Givarch A 1994 *J. Alloys Compd.* **206** 21

[39] Holseth H and Kjekshus A 1968 *Acta Chem. Scand.* **22** 3273

[40] Wilson A 1938 *Proc. Roy. Soc. Lond. A* **167** 580

[41] Webb G W 1969 *Phys. Rev.* **181** 1127

[42] Babizhetskyy V, Kotur B, Oryshchyn S, Zheng C, Kneidinger F, Leber L, Simson C, Bauer E and Michor H 2013 *Solid State Commun.* **164** 1

[43] Zeppenfeld K and Jerrschko W 1993 *J. Phys. Chem. Solids* **54** 1527